THE REMOVAL OF LIGANDS FROM COLLOIDAL NANOCRYSTAL FILMS WITH HE AND O2 PLASMAS IS LIMITED BY MASS TRANSPORT AND CROSSLINKING

Journal:	*Physical Chemistry Chemical Physics*
Manuscript ID	CP-ART-11-2018-006890.R1
Article Type:	Paper
Date Submitted by the Author:	12-Dec-2018

Complete List of Authors:	Shaw, Santosh; Iowa State University, Materials Science and Engineering Silva, Tiago; University of São Paulo, Institute of Physics Mohapatra, Pratyasha; Iowa State University Mendivelso-Perez, Deyny; Iowa State University, Chemistry Department Tian, Xinchun; Iowa State University, Ludovico Cademartiri Naab, Fabian; University of Michigan , Michigan Ion Beam Laboratory Rodrigues, Cleber; University of São Paulo, Institute of Physics Smith, Emily; Iowa State University, Dept of Chemistry Cademartiri, Ludovico; Iowa State University, Materials Science & Engineering

ON THE KINETICS OF THE REMOVAL OF LIGANDS FROM FILMS OF COLLOIDAL NANOCRYSTALS BY PLASMAS

SANTOSH SHAW[1], TIAGO F. SILVA[2], PRATYASHA MOHAPATRA[1], DEYNY MENDIVELSO-PEREZ[3], XINCHUN TIAN[1], FABIAN NAAB[4], CLEBER L. RODRIGUES[2], EMILY A. SMITH[3], LUDOVICO CADEMARTIRI[1,5,6,*]

[1]*Department of Materials Science & Engineering, Iowa State University of Science and Technology, 2220 Hoover Hall, Ames, IA, 50011*
[2]*Instituto de Física da Universidade de São Paulo, Rua do Matão, trav. R 187, 05508-090 São Paulo, Brazil*
[3] *Department of Chemistry, Iowa State University of Science and Technology, Gilman Hall, Ames, IA, 50011*
[4] *Michigan Ion Beam Laboratory, University of Michigan, 2600 Draper Road, Ann Arbor, MI 48109, USA*
[5]*Department of Chemical & Biological Engineering, Iowa State University of Science and Technology, Sweeney Hall, Ames, IA, 50011*
[6]*Ames Laboratory, U.S. Department of Energy, Ames, IA, 50011*

[*] *Author to whom correspondence should be addressed: lcademar@iastate.edu*

ABSTRACT

This paper describes the kinetic limitations of etching ligands from colloidal nanocrystal assemblies (CNAs) by plasma processing. We measured the etching kinetics of ligands from a CNA model system (spherical ZrO_2 nanocrystals, 2.5-3.5 nm diameter, capped with trioctylphosphine oxide) with inductively coupled plasmas (He and O_2 feed gases, powers ranging from 7 to 30W, at pressures ranging from 100 to 2000 mTorr and exposure times ranging between 6 and 168 hrs). The etching rate slows down by about one order of magnitude in the first minutes of etching, after which the rate of carbon removal becomes proportional to the third power of the carbon concentration in the CNA. Pressure oscillations in the plasma chamber significantly accelerate the overall rate of etching. These results indicate that the rate of etching is mostly affected by two main factors: (i) the crosslinking of the ligands in the first stages of plasma exposure, and (ii) the formation of a boundary layer at the surface of the CNA. Optimized conditions of plasma processing allow for a 60-fold improvement in etching rates compared to the previous state of the art and make the timeframes of plasma processing comparable to those of calcination.

INTRODUCTION

The application of colloidal nanocrystals in devices requires, in most cases, their conversion to solid state, fully inorganic materials[1-7]. We[8-12], and others[13-18], have been interested in resolving this problem to enable the bottom-up manufacturing of materials with designed microstructure and interfaces and therefore with unique and predictable mechanical, electrical, and optical properties.

The conversion of CNAs into solid state all-inorganic materials is notoriously troublesome, especially if the desired product is a single phase: it is difficult to remove completely the ligands, especially without compromising the size and shape of the nanocrystals (e.g., coarsening), their surface composition (e.g., oxidation), and the structure of the CNA (e.g., cracking). The particularly challenging nature of the problem arises due to (i) the large volume fraction of organic matter in CNAs (usually between 30 vol% and 60 vol%, and often significantly more due to incompletely purified colloids), (ii) the nano/mesoporous structure of CNAs, which greatly limits mass transport[12, 19], (iii) the weak interactions between the colloids[20], which reduces the tolerance to strains during ligand removal, and (iv) the high surface energy of the bare colloids, which increases their reactivity and facilitates their growth[21].

Calcination is one of the most common strategies for the removal of organics from nanostructured materials. The process is usually conducted in static air or O_2 atmosphere, at temperatures ranging from 300°C to 800°C for various amounts of time, but often less than 1 hr[22]. This process is not compatible with organic substrates, or with materials that are susceptible to oxidation. Most nanostructured phases coarsen significantly upon exposure to the high temperatures of calcination[23], which can compromise their size-dependent properties[24]. Furthermore, as recently shown, calcination does not remove all carbon from CNAs, leaving behind between 20% and 40% of the original carbon atoms (depending on calcination temperature) in the form of amorphous carbon[12].

Ligand stripping or replacement is another very common strategy that involves the washing of CNAs with a chemical that strips ligands off[25] or with a competing ligand that replaces the ones previously bound[26]. This approach was used successfully to reduce the distance between nanoparticles in films to allow for electron transport[27]. This approach does not usually remove all organics[28] and induces large capillary stresses which lead to cracking of the films[29].

The use of inorganic ligands is an elegant approach[1, 30], by which nanoparticles are coordinated and colloidally stabilized by inorganic groups. The ultimate flexibility of this approach is not yet established and in many cases yields composites rather than phase pure materials.

Plasmas have been shown to selectively remove ligands from nanoparticles monolayers at least since 2005[14, 31]. Early work from those same years showed that CNAs with as many as ~100 layers of nanoparticles (PbS[11], Bi_2S_3[32], $CoFe_2O_4$[33]) could be processed by plasmas and that the removal of ligands would also take place inside the CNA.

Plasmas (Figure 1) – a complex, out-of-equilibrium gas phase produced by the acceleration of volatile charged species (electrons and ions) by an externally applied electromagnetic field – are well known as etchants for organics as well as inorganics[34-36]. They comprise various species, i.e., electrons, ions, photons (from the vacuum ultraviolet range (VUV), 10-200nm, to the visible range), radicals, excited molecules, and atoms. The concentration and the kinetic energy of these species strongly depend on the pressure, the power and frequency of the electromagnetic field, the composition of the feed gas, and the geometry of the electrodes (e.g., capacitive vs inductive).

The plasma environment can interact with materials in multiple ways, especially if the material is porous, such as a CNA (Figure 1). Accelerated ions can ablate surfaces and implant into them. Ions and electrons have relatively large mean free paths (easily of hundreds of μm) and are typically neutralized on solid surfaces[37]. The penetration depths for ions are in the order of nanometers. Radicals/excited species are the longest-lived excited species in the plasma and can instead

penetrate porous materials by free molecular diffusion. Photons can also penetrate significantly in materials by transmission. Vacuum ultraviolet (VUV) radiation (10-200nm) is heavily absorbed by saturated polymer chains[38], and has sufficient energy (124eV–6eV) to break C-C bonds[39, 40], but require reactive gases to yield stable volatile species that can be removed in the vacuum of the plasma[37, 41]. At wavelengths smaller than 120nm, the energy of the photons (~10eV) is sufficient to ionize organic molecules[38]. Organic byproducts of plasma etching can react further in the plasma environment, where they can repolymerize and redeposit, by a process called "plasma polymerization"[42].

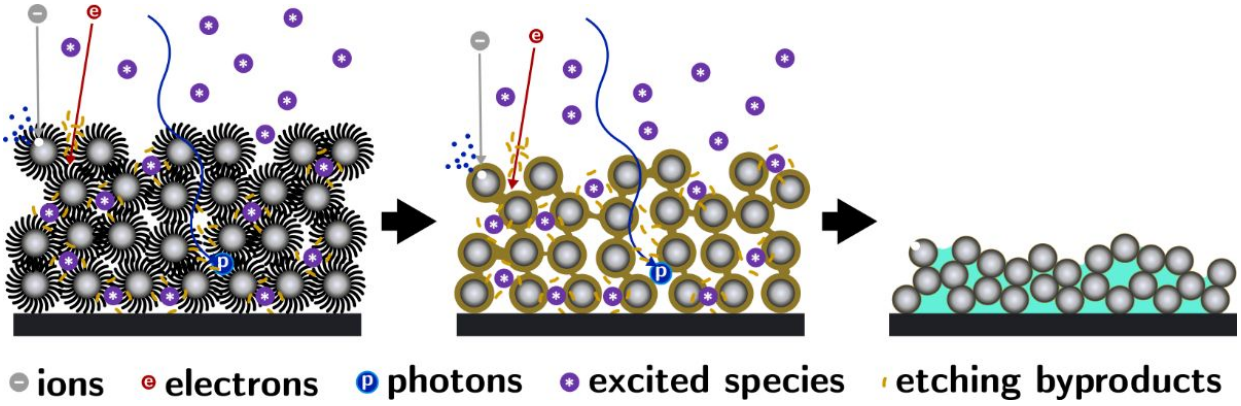

Figure 1. Schematics of the interactions between plasmas and colloidal nanocrystal assemblies (CNA). Plasma-generated ions, electrons, photons, and neutral excited species penetrate to different extents in the porous network formed by the CNA. Prior data suggest an open structure is formed at intermediate stages of etching.

In our previous work we investigated the interactions of plasmas with CNAs. Due to the variety of parameters that control the reactivity of plasmas (e.g., pressure, concentration of active species, temperature, chemical reactivity and ablative power of the active species, EM field geometry, power and frequency) and CNAs (which vary in terms of porosity, organic fraction, pore size, surface reactivity, propensity to grain growth, etc…), we used a model system consisting of CNAs (200-450 nm thick films on Si substrates) of ZrO_2 nanocrystals (spherical shape, 2.5-3.5 nm diameter, capped

with trioctylphosphine oxide) and an inductively coupled plasma (Harrick plasma cleaner PDC-001, powers ranging from 7 to 30W, at pressures ranging from 100 to 2000 mTorr and exposure times ranging between 6 and 168 hrs).

Our prior work has shown that:

(i) O_2 plasmas can reduce the concentration of carbon below 1 at%, in a homogeneous process that yields no compositional gradients across the thickness of the CNA (between 180 nm and 250 nm)[8]. Zr, O, P, and Cl are preserved during etching with either O_2 or He. No particle coarsening was observed[43].

(ii) The removal of the ligands by plasma does not induce cracking as long as the CNAs are disordered and thinner than 400-450nm[9]. The volume loss occurs unidirectionally, perpendicularly to the substrate. The vertical collapse of the CNA occurs in two phases: the pore volume of the nanocrystal array increases initially from 25% to 54% and then decreases to 38% in the fully processed film. The initial increase in porosity was attributed to the formation of "necks" between the particles[8], while the final decrease in porosity was attributed to the etching of the necks between the particles.

(iii) Non-oxidizing feed gases like He can remove ligands from oxygen-sensitive CNAs (PbS[44] or Si[45]). This approach was used to create PbS films from PbS CNAs in one step. Our work further showed that He plasma (like O_2 plasmas) remove ligands mostly by the action of excited species, rather than by high energy photons[44] .

This present study identifies the factors that reduce the rate of removal of ligands from CNA by plasma processing, by conducting an extensive kinetic study on etching rates using Elastic Backscattering (EBS) and Elastic Recoil Detection (ERD)[46-48]. We find that etching is partially limited by mass transport due to the formation of a boundary layer at the surface of the CNA (diffusion inside the CNA, albeit drastically slowed by confinement, is not rate limiting due to the

thickness of the film). Also, the reduction of the rate of etching over the course of the process is consistent with the progressive crosslinking of the ligands as a result of reaction with diffusing radicals and exposure to UV/VUV radiation generated by the plasma. We further show how the rates of etching depend on plasma pressure, plasma power, and feed gas and can be accelerated by ~60 times compared to the previous state of the art conditions by appropriate optimization.

EXPERIMENTAL DESIGN

We used CNAs (thickness before etching: ~350nm) made from ZrO_2 nanoparticles (~3nm diameter, ligand: trioctylphosphine oxide – TOPO, cf. Figure 2a). These films are an excellent model system for the study of the influence of plasma species on CNAs for the following reasons. ZrO_2 is an important and extensively studied functional oxide material for its mechanical, thermal, and catalytic properties. It is a very strong lattice that is resistant to ablation and impervious to oxidation. The particles can be easily synthesized at a gram scale. They are also extremely stable as colloids. This stability allows us to clean them extensively (therefore reducing to a minimum the concentration of free, unbound ligands) and to deposit them as relatively thick films (up to 500 nm) in one step by spin-coating from highly concentrated dispersions (up to 400 mg/ml[9]). The small size of the particles makes them an excellent model for testing mass transport limitations in the etching of ligands by plasmas.

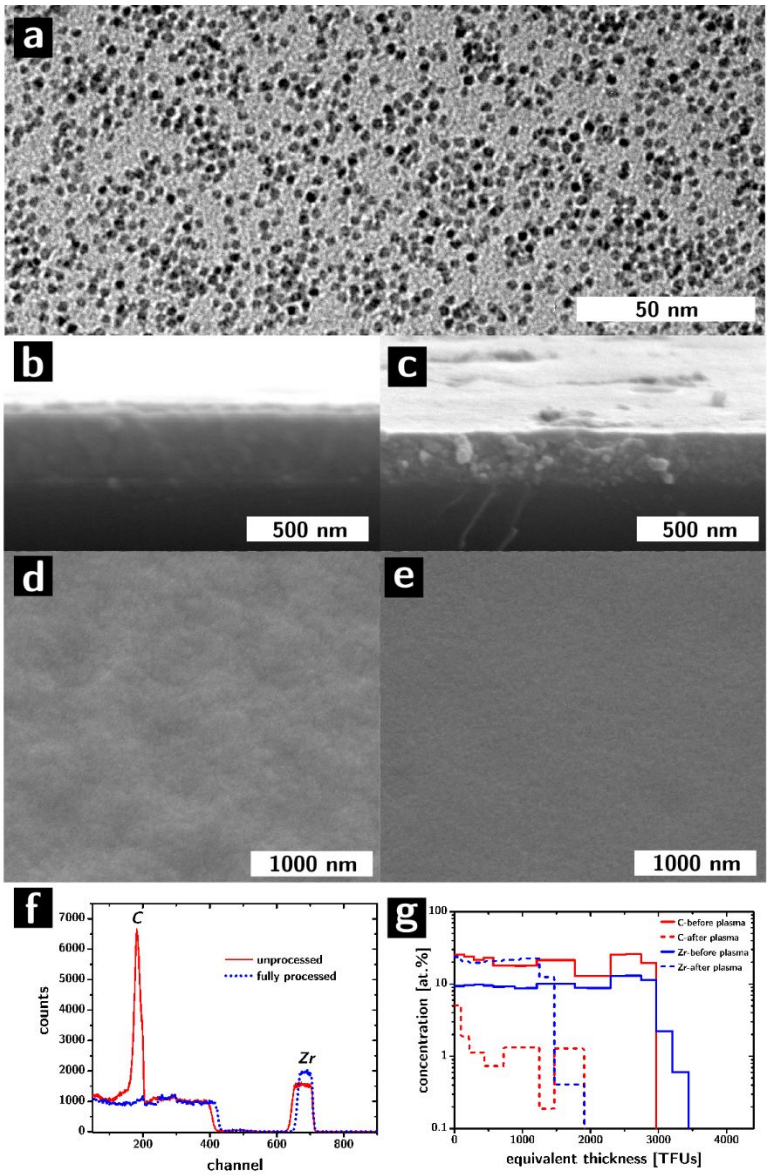

Figure 2. (a) TEM micrograph of the purified colloidal ZrO_2 nanocrystals. Cross-sectional **(b-c)** and top **(d-e)** views of the films before **(b,d)** and after **(c,e)** ligand removal by plasma processing. **(f)** Raw EBS spectra of the ZrO_2 CNAs before (red line) and after (blue line) plasma processing. **(g)** Concentration profile for Zr (blue) and C (red) in the CNAs before (continuous lines) and after (dashed lines) plasma processing. 0 TFU corresponds to the film surface.

The synthesis of the nanoparticles was performed as previously reported[9] and the particles were deposited from highly concentrated (~100 mg/ml) hexane dispersions to form 350-nm-thick disordered CNAs that would not crack upon ligand removal (cf. Figure 2b-e), as previously discussed[9].

It is impossible to characterize the interactions of all types of plasmas with colloidal nanoparticles. Therefore, we focused this extensive study on the range of parameters and the type of plasma (inductively coupled) that is most commonly used for removing ligands from CNAs. In order to identify the rate-limiting step of etching, we characterized the carbon concentration in the CNAs as a function of processing time (0, 1 min, 10 min, 1 hr, and 6 hr), plasma pressure (from 100mTorr to 2000mTorr), power (7W and 30W), and feed gas (He or O_2).

These parameters were chosen for their key role in determining the energy, concentration, and composition of the species composing the plasma. Plasma power linearly affects the energy and density of plasma species[38, 41, 49]. The pressure in the chamber also controls the density of plasma species[50, 51] and their mean free path[49, 50]: at lower pressures (<100mTorr) the mean free path is larger (less collision opportunities), leading to fewer species with higher energy; at higher pressures, the mean free path of electrons is shorter, which leads to lower kinetic energies (i.e. reduced electron temperature), and again fewer reactive species (due to the lower probability of ionization in response of collisions). Photon density decreases at higher pressures due to the lower kinetic energy of electrons, and the increased rate of self-absorption due to higher concentration of the gas, especially in the case of O_2 plasmas[37]. The feed gas determines the composition, density, and energy of the active species. O_2 plasma aggressively etches organics[38, 52] by (i) radical site generation by oxygen radicals and photons, (ii) formation of oxidative derivatives by reactions with oxygen atom/molecules/radicals, and, finally, (iii) scission to form volatile products like CO, CO_2, ROOH, ROH, ROO, etc… On the other hand, it shows a rather sparse and weak UV emission spectrum

and some strong VUV emission[52] which can also contribute to etching. He plasmas instead have a much stronger emission in both the UV and VUV range and, while they can produce radicals through the reaction of He metastable species with organics, they are chemically less reactive towards organics than an O_2 plasma[52]. The etching of organics by He plasma is thought to be caused by helium metastable species and VUV, through the generation of hydrocarbon and hydrogen radicals, which can then reacts to form H_2 or volatile species[53]. The release of H_2 in the plasma can have a disproportionate effect on its VUV emission [52] as well as on the etching chemistry[41].

As in our previous study, we opted to characterize the concentration of carbon in the films by the use of EBS and ERD, as they allow the simultaneous quantification of all elements in the films (in TFUs, thin film units, defined as 10^{15} atoms/cm^2), across the entire thickness of the films. Modeling of all spectra (see Supporting Information) allowed us to further reconstruct the concentration of each element as a function of depth into the films. While this characterization is undoubtedly cumbersome and extremely time consuming, these techniques are necessary to obtain quantitative characterization of carbon at such low concentrations and in a depth-dependent manner over hundreds of nanometers.

RESULTS AND DISCUSSION

Optimized plasma processing parameters allow ligand removal in 6 hrs

Figure 2f shows the EBS spectrum collected from ZrO_2 films processed by O_2 plasma at 30W, and 500 mTorr for 6 hrs, as compared to the spectrum of the unprocessed film. The peak of carbon (at channel ~200) is noticeably reduced upon exposure to the plasma. Figure 2g shows the reconstructed depth profiles of the concentrations of C (red) and Zr (blue), before (continuous line) and after (dashed line) plasma processing. The concentration of carbon after processing is approximately constant at ~1 at% throughout the thickness of the material. The apparent increase

in the concentration of Zr after processing is due to the normalization to atomic percentages. The absolute amount of Zr was not found to be significantly affected by plasma processing (273±30 TFU before plasma vs 251±30 TFU after plasma, and the error originates from thickness variations between samples and is calculated as 95% confidence interval). These data demonstrate that plasmas can remove the majority of organics from CNAs in times comparable to calcination and shorter than an overnight period.

Etching rates depend strongly on time

Figure 3a is a log plot of the concentration of carbon (in TFUs, as obtained by EBS/ERD characterization) as a function of processing time for all the plasma processing parameters we tested. In all conditions, most of the carbon is removed in the early stage of plasma processing. The color coding of the scatters (black for He plasmas, red for O_2 plasma) shows that the feed gas is the dominant parameter in determining the etching kinetics.

Fitting the curves allows a more quantitative comparison of the influence of the feed gas on the etching kinetics and provides some additional insight. The He and O_2 datasets were fit with exponential decays (R^2=0.97 and 0.82 for He and O_2 datasets respectively) with time constants equal to 11000±2000 s and 3000±1000 s (error indicates 95% confidence interval) for He and O_2 datasets respectively, indicating the slower etch rates for He plasma. Interestingly, the fits required an offset in the concentration suggesting that neither feed gases would reduce carbon concentrations below 44 TFUs. We hypothesize that this offset does not indicate a limitation of the plasma processing itself but that is rather a side effect of the deposition of adventitious carbon (plausibly in the form of carbonates[54] and other organics) into the films after their removal from the plasma chamber. 44 TFUs of carbon could be accounted for by much less than a monolayer coverage of the surfaces in a ligand-free CNA. This hypothesis is further consistent with our prior findings that samples processed for 168 hr showed similar residual carbon concentrations.

Figure 3b shows the rates of etching in units of TFU/s as a function of processing time, in a log-log format, for all the processing conditions we tested. The data were obtained by dividing the changes in TFU shown in Fig. 3a by the time interval over which they occurred. As in the case of Figure 3A, we color-coded the scatters to identify the different feed gases. While this plot might suggest that O_2 plasmas decrease in effectiveness sooner than He plasmas, the amount of carbon still in the film is different for the two feed gases after the same time of processing. Nonetheless, the etch rates decrease by order of magnitudes over the course of the ligand removal for all plasma parameters we tested. This striking result strongly suggests that the process is kinetically hindered.

Etching rates depend with the third power of the residual carbon concentration

Etching is a chemical process whose rate is expected to depend on the concentration of the reactants. If we assume that the concentration of etchants (i.e., the excited species in the plasma) is constant during processing, the rate of etching should be expressed by a rate equation of the form:

$$\frac{\partial[C]}{\partial t} = -k[etchant] = -k^{'}[C]^{n}$$

Where n is the order of the reaction and k' is a rate constant.

Therefore, plots of the etching rates as a function of the concentration of carbon in the CNAs should allow for the estimation of k' and n, and how these two constants depend on the plasma parameters (i.e., pressure, power, feed gas). The data is shown in Figure 3c as a log-log plot.

The plot shows that both feed gases start the processing (top right, high [C]) with similar, very high values of etch rates (~1 TFU/s). Both drop significantly (He more so) after the first 10-20% of the carbon is removed. After this initial stage, the etch rate appears to depend on [C] as a power law with strikingly similar exponents (i.e., slopes in the log-log plot) for both feed gases. Both trends can be very well fit with a power law with an exponent $n = 3$.

This exponent in the rate equation defines the average order of the etching reaction and, therefore, carries significant information about its mechanism. A third order of reaction suggest that, on average ~3 chain scission events must occur simultaneously and in close proximity to each other for carbon to be removed from the system. This interesting observation suggests the hypothesis that this slowdown in the rate of etching could be due to the crosslinking of the ligands. The delayed onset of this third order dependence on [C] is consistent with crosslinking being a side-effect of the exposure of the films to UV/VUV radiation and radical-generating species. The fact that the exponent is the same for two feed gases that operate through completely different reaction mechanisms also suggests that this third order kinetic is not due to the etchant (O_2 and He plasmas) but rather due to the organic fraction. The only similarity between the two feed gases is their potential for crosslinking of organics due to their UV emission.

Etch rate constants depend mostly on feed gas and pressure

If we assume that (for anything but early stage etching) the rate law is truly of the third order, we can extract the rate constants *k'* for different plasma etching parameters, e.g., O_2 vs He plasmas, 7W vs 30W, 100mTorr vs 500mTorr vs 2000mTorr. The results are shown in Figure 3d.

The average rate constant for O_2 plasmas is nearly an order of magnitude larger than for He plasmas ($2.69 \cdot 10^{-9} \pm 0.38 \cdot 10^{-9}$ $TFU^{-2}s^{-1}$ vs $0.388 \cdot 10^{-9} \pm 0.26 \cdot 10^{-9}$ $TFU^{-2}s^{-1}$). Interestingly, an increase in power by a factor of 4.3 only leads to a marginal increase in the rate constant ($1.47 \cdot 10^{-9} \pm 0.34 \cdot 10^{-9}$ $TFU^{-2}s^{-1}$ vs $1.75 \cdot 10^{-9} \pm 0.31 \cdot 10^{-9}$ $TFU^{-2}s^{-1}$), which is within the 95% confidence interval. This is surprising since power affects the concentration of the active plasma species and their energy.

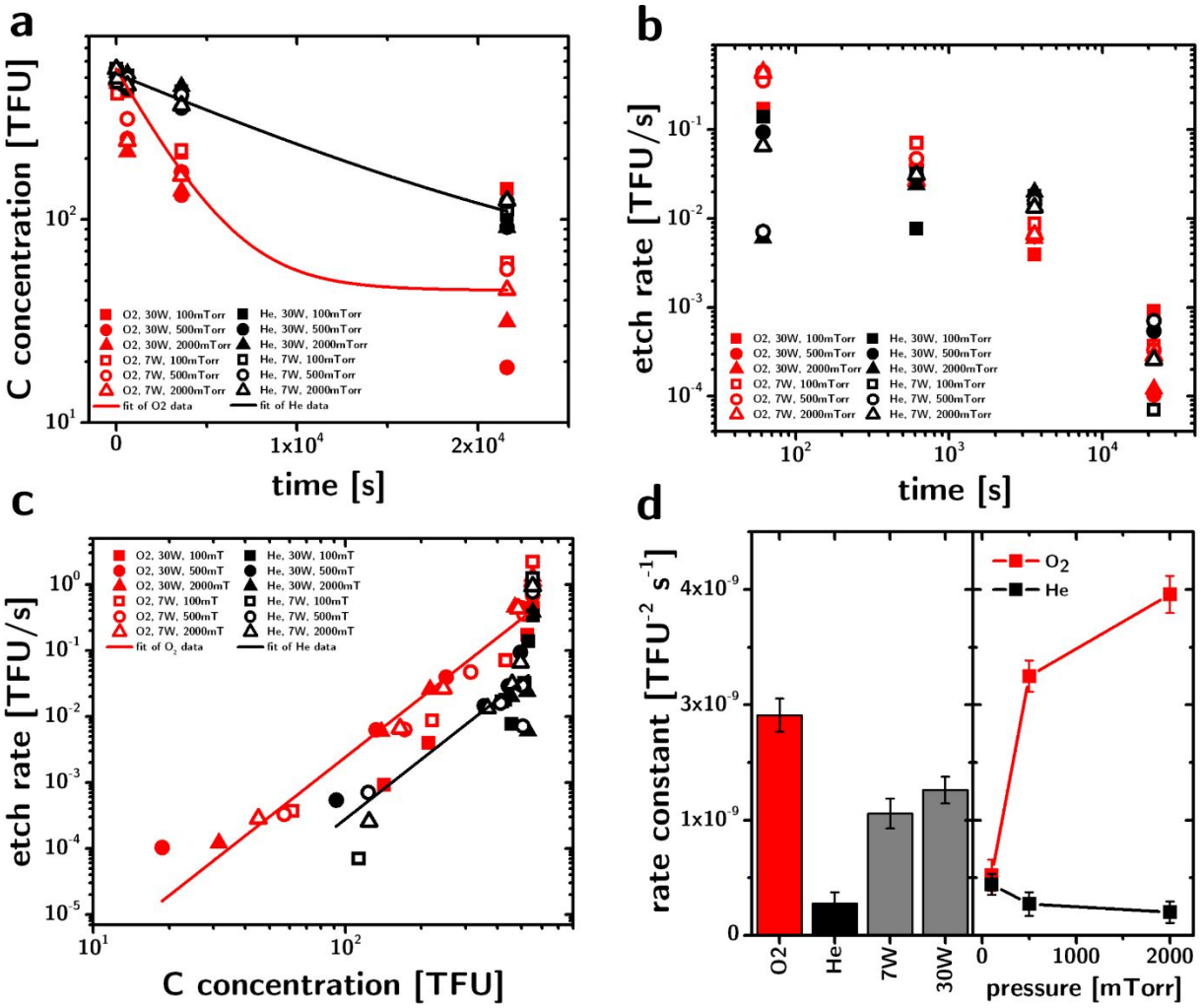

Figure 3. Kinetic analysis of ligand etching as a function of plasma parameters (O_2, red scatters; He, black scatters; 30W, filled scatters; 7W, open scatters; 100mTorr, squares; 500mTorr, circles; 2000mTorr, triangles). **(a)** Carbon concentration in thin film units (TFUs) as a function of processing time. **(b)** Carbon etching rates (in units of TFUs/s) as a function of processing time. **(c)** Carbon etch rates in TFUs/s as a function of carbon concentration in TFUs. **(d)** Rate constants of ligand etching calculated from the straight lines in panel (c) for different classes of plasma parameters.

Pressure has, instead, a significant impact on the average rate constants. In the case of O_2 plasmas, a 20-fold increase in pressure from 100mTorr to 2000mTorr, increased the average etching rate constant nearly 6-fold ($0.73 \cdot 10^{-9} \pm 0.36 \cdot 10^{-9}$ $TFU^{-2}s^{-1}$ vs $4.11 \cdot 10^{-9} \pm 0.43 \cdot 10^{-9}$ $TFU^{-2}s^{-1}$). For He, instead, the same 20-fold increase in pressure caused a 2-fold decrease in the average etching rate constant ($0.62 \cdot 10^{-9} \pm 0.24 \cdot 10^{-9}$ $TFU^{-2}s^{-1}$ vs $0.28 \cdot 10^{-9} \pm 0.25 \cdot 10^{-9}$ $TFU^{-2}s^{-1}$). This difference in the influence of pressure on the average etching rate is consistent with the differences in the etching mechanisms of two feed gases. The dominant etching mechanism in O_2 plasmas is the oxidation by reactive oxygen species, especially radicals, whose concentration increases significantly with increasing pressure. The dominant etching mechanism in He plasmas is instead due to reactive He species which require very high energies collisions to form, and, therefore, are promoted by a decrease in pressure and the associated increase in the mean free path. Furthermore, lower pressures reduce the self-absorption of UV and VUV radiation that contributes significantly to the etching in He plasmas.

Significantly, the rate constants for O_2 and He plasmas are nearly equivalent at 100mTorr, indicating that a combination of low pressures (<100mTorr) and high powers (≥30W) could make He plasmas as effective as O_2 plasmas.

Etching is limited by mass transport, but not within the films

The extremely fast decrease in etch rates with time suggests that etching could be also kinetically limited by the production of volatile etching byproducts. These volatiles could (i) fill the pores of the CNAs and prevent diffusion of reactive species from the plasma into the CNA, and (ii) form a byproduct-rich boundary layer at the surface of the film, also preventing reactive plasma species from accessing the CNA.

Chemical reactions in porous media are often diffusion limited. For example, the burnout of binders from ceramic powders is still a major challenge in ceramic powder processing[55]. The calcination of

ceramic powders often leaves behind significant organic contamination in spite of the relatively large (μm to mm) size of the particles and the relatively small volume fraction of binder that must be removed (especially when compared to CNAs where a ~50% volume fraction of organics must be removed from nanoscale pores). As we have shown in a recent publication, this same problem occurs in the calcination of CNAs[12].

Diffusion of gaseous molecules in the samples we measured occurs in the regime of free molecular diffusion (Knudsen regime), whereby the mean free path of the gaseous molecule l ($5.84 \cdot 10^{-4}$ m for O at 300K and 100mTorr) is much larger than the pores size p ($\sim 1 \cdot 10^{-9}$ m). The Knudsen number $K_n = l/p$ is $\sim 10^5$ in our system. For $K_n \gg 1$, the gas molecules interact almost exclusively with the walls of the system rather than with other gas molecules. As a result, the diffusivity is significantly reduced, when compared to molecular diffusion conditions. The Knudsen diffusivity $D_{\{KA\}}$ in our system can be estimated by two formalisms to be $0.635 \cdot 10^{-7}$ m^2s^{-1} or $2.17 \cdot 10^{-7}$ m^2s^{-1} rather than the molecular diffusivity value of $1.23 \cdot 10^{-1}$ m^2s^{-1}. The first formalism is basic and considers cylindrical pores and expresses $D_{\{KA\}}$ as

$$D_{\{KA\}} = \frac{d}{3}\sqrt{\frac{8RT}{\pi M_A}}$$

Where d is the pore diameter and MA is the molecular mass of the diffusing gas. The second formalism accounts for tortuosity, spherical particle shape, and total porosity and expresses $D_{\{KA\}}$ as

$$D_{\{KA\}} = \frac{\pi \quad \phi \quad \upsilon r}{8 + \pi 1 - \phi\ \tau}$$

Where ϕ is porosity, τ is the tortuosity (a geometric, dimensionless parameter that accounts for the increase in path length due to tortuous pores), ν is the mean gas velocity, and r is the particle radius.[56]

In our system it is fair to assume that the pores are accessible due to (i) the spherical shape of the particles in the films, and (ii) the evidence of homogeneous and near-complete removal of organics throughout the thickness of the films.

The reduction by six orders of magnitude of the diffusivity could suggest that etching is indeed diffusion limited inside the CNA. And yet, this conclusion would be contradicting the evidence we presented in Figure 2g (and in prior publications[57]) for homogeneous etching across the thickness of the CNA. A closer look at the numbers shows that, even assuming diffusivities in the order of 10^{-7} m^2s^{-1} as calculated above, the diffusion inside the film would not be rate-limiting simply because the films are very thin. Considering 350 nm films containing 500 TFU of carbon (in the form of volatile species), and surrounded by air devoid of carbon, the flow of carbon out of the film into the environment (assuming a diffusivity inside the film of D=$\sim 10^{-7}$ m^2s^{-1}, as calculated above) would be $\sim 10^{-21}$ $m^{-2}s^{-1}$. All the 500 TFU of carbon originally in the film could diffuse out of the film in the span of few seconds, a much shorter time than our processing time. On the basis of these arguments and the experimental evidence mentioned before, we hypothesized that diffusion within the CNAs, even though drastically slowed by confinement, is not a rate limiting factor (at least in the processing conditions explored so far). These observations also imply, importantly, that the pores in the CNAs should not be filled with excess ligands for plasma etching to be effective.

Diffusion could still be kinetically limiting through the formation of a stationary boundary layer composed of highly concentrated etching byproducts. We simulated (cf. Supporting Information) the mass transport in the plasma chamber (cf. Figure 4). Figure 4a shows the gas velocity (assumed to be pure O_2) inside the chamber. The inset shows the volume of fluid above the sample, showing the formation of a boundary layer at the sample surface. To estimate the influence of this boundary layer on the local concentration of plasma species, we assumed that the CNA top surface would act as a source of gas (CO_2) at a rate equal to the maximum etch rate measured in our experiment (10^{-1}

TFU/s). The concentration of etching byproducts in proximity of the sample surface is shown in Figure 4b, showing the accumulation of byproducts caused by the boundary layer.

These simulations suggest that the boundary layer could effectively slow down the rate at which active plasma species can enter the CNA. To test this hypothesis experimentally we applied a similar approach to the one originally proposed by Cima and colleagues to circumvent the mass transport limitations in binder burnout[55]: pressure oscillations. By exposing the system to oscillatory pressures the boundary layer is disrupted and the film is emptied of reaction byproducts and recharged with reactive species.

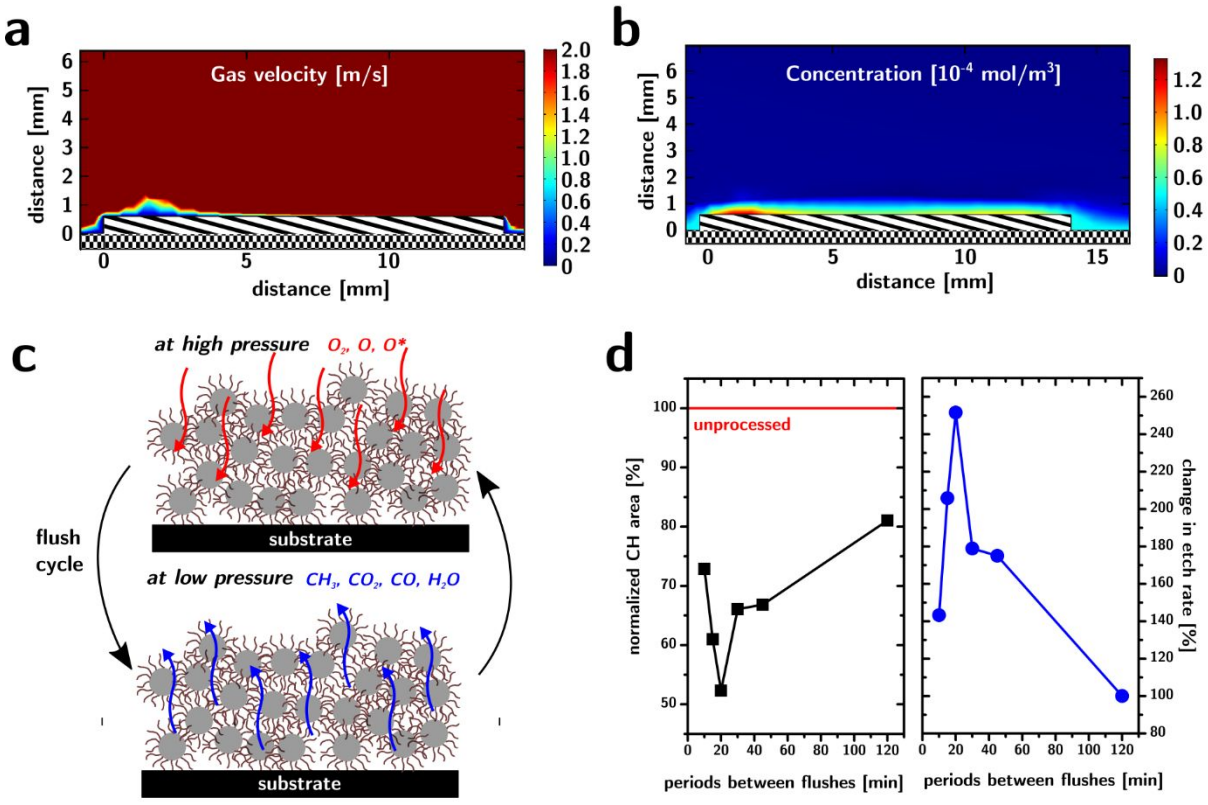

Figure 4. Boundary layer as a limiting factor in ligand etching by plasmas. (a) Side view of the gas velocity in the plasma chamber above the substrate (shown with diagonal lines) and the sample holder (shown with a checkerboard pattern). **(b)** Side view of the concentration of etching byproducts above the substrate, showing

the existence of a boundary layer of ~600 μm. **(c)** Schematic depiction of the mechanism of action of pressure oscillations in ameliorating the effect of boundary layers. **(d)** Area of the C-H stretching modes in Raman spectroscopy from films processed with different time intervals between pressure oscillations. The peak areas are normalized to those of the unprocessed film. By assuming a roughly linear dependence between peak area and carbon concentration, the dependence of the etching rate on the time period between pressure oscillations is shown on the right.

We exposed films to a total of 2 hr of plasma etching at 30 W and 500 mTorr. After a time of processing τ, the plasma chamber was evacuated (100 mTorr), and then returned to the original pressure conditions with fresh feed gas. The plot in Figure 4d shows the amount of carbon in the films (quantified by the integrals of the peaks associated with C-H stretching modes in Raman spectroscopy) for different values of τ. The data show that when the time τ between evacuations is 20 minutes, the integrals of the C-H signals are half of those of the samples treated without evacuations, indicating an overall increase of the rate of etching by a factor of 2. Longer times, or shorter times showed smaller improvements of etch rates, consistent with the formation of a diffusion barrier at the film surface.

CONCLUSIONS

In this work we have determined, through an extensive characterization of carbon concentrations by ion beam analysis techniques, the kinetics of the plasma etching of organic ligands from model colloidal nanoparticle assemblies composed of ZrO_2 nanocrystals. It is important to note that these findings were obtained from colloidal nanocrystal films that were porous upon their deposition thanks to the removal of excess ligands from the nanocrystal dispersion through extensive purification. Lack of porosity in the as-deposited films (which can result from using nanocrystal

dispersions with significant amounts of excess ligands) is expected to significantly affect the kinetics of etching and will be subject of a follow-up study.

Our data indicates that etching takes place in two distinct phases. The first phase (during which the first 20-25% of the original carbon is removed) lasts a very short time (1-10 min), during which the etch rates are very large ($\sim 10^{14}$ atoms·cm^{-2}·sec^{-1}), but drop rapidly with time and with the remaining carbon concentration. In the following phase, which appears to last till the end of processing, the rates of etching decrease less rapidly and proportionally to the third power of the concentration of remaining carbon (regardless of feed gas, plasma power, or pressure), suggestive of crosslinking of the carbon network.

This kinetics allowed the estimation of rate constants in this second phase and their dependence on plasma processing parameters. We found that O_2 plasma are faster than He plasmas, on average, by nearly an order of magnitude. Power, on the other hand, had a very small effect (between 7W and 30W). Pressures had a large effect on rate constants, but with opposite trends for O_2 and He plasmas: higher pressures (e.g., 2000mTorr) led to higher rate constants for O_2, and lower rate constants for He. At 100mTorr the rate constants for O_2 and He plasmas were comparable.

As a result of this study we found conditions in which the organics from CNAs could be effectively removed in as short a time as 6 hrs, compared to the 168 hrs reported before. Importantly we have identified a strategy that could further accelerate etching without necessarily leading to significant ablation: using He feed gas at pressures below 100mTorr and powers well above 30W;

An analysis of the mass transport in the plasma chamber by simulation and modeling indicates that mass transport is reduced inside the CNA due to confinement, but it is not limiting the etching rate. On the other hand, diffusion at the surface of the CNAs, where a boundary layer develops, is indeed limiting, as was demonstrated by a oscillatory pressure experiment that allowed us to improve etch rates by a factor of two by disrupting the accumulation of etching byproducts at the CNA.

In summary these result establish a framework for the understanding of the rate limiting factors in the etching of organic ligands from CNAs using plasmas, and suggest that bulk quantities of materials could be processed if crosslinking of the organic fraction could be avoided.

ACKNOWLEDGMENTS

The work described in this paper has been supported by the Member-Specific-Research-Intel program of Semiconductor Research Corporation under Award No. 2015-IN-2582. Preliminary work was funded by Iowa State University through a startup grant to L.C. The Raman measurements were supported by the U.S. Department of Energy, Office of Basic Energy Sciences, Division of Chemical Sciences, Geosciences, and Biosciences through the Ames Laboratory. The Ames Laboratory is operated for the U.S. Department of Energy by Iowa State University under Contract No. DE-AC02-07CH11358

REFERENCES

1. D. S. Dolzhnikov, H. Zhang, J. Jang, J. S. Son, M. G. Panthani, T. Shibata, S. Chattopadhyay and D. V. Talapin, *Science*, 2015, **347**, 425-428.
2. M. V. Kovalenko, L. Manna, A. Cabot, Z. Hens, D. V. Talapin, C. R. Kagan, V. I. Klimov, A. L. Rogach, P. Reiss, D. J. Milliron, P. Guyot-Sionnnest, G. Konstantatos, W. J. Parak, T. Hyeon, B. A. Korgel, C. B. Murray and W. Heiss, *ACS Nano*, 2015, **9**, 1012-1057.
3. M. V. Kovalenko, R. D. Schaller, D. Jarzab, M. A. Loi and D. V. Talapin, *J. Am. Chem. Soc.*, 2012, **134**, 2457-2460.
4. J. Tang, K. W. Kemp, S. Hoogland, K. S. Jeong, H. Liu, L. Levina, M. Furukawa, X. H. Wang, R. Debnath, D. K. Cha, K. W. Chou, A. Fischer, A. Amassian, J. B. Asbury and E. H. Sargent, *Nat. Mater.*, 2011, **10**, 765-771.
5. G. Konstantatos, I. Howard, A. Fischer, S. Hoogland, J. Clifford, E. Klem, L. Levina and E. H. Sargent, *Nature*, 2006, **442**, 180-183.
6. R. Tangirala, J. L. Baker, A. P. Alivisatos and D. J. Milliron, *Angew. Chem.*, 2010, **122**, 2940-2944.
7. E. L. Rosen, R. Buonsanti, A. Llordes, A. M. Sawvel, D. J. Milliron and B. A. Helms, *Angewandte Chemie International Edition*, 2012, **51**, 684-689.
8. S. Shaw, J. L. Colaux, J. L. Hay, F. C. Peiris and L. Cademartiri, *Advanced Materials*, 2016, **28**, 8900-8905.

9. S. Shaw, B. Yuan, X. C. Tian, K. J. Miller, B. M. Cote, J. L. Colaux, A. Migliori, M. G. Panthani and L. Cademartiri, *Advanced Materials*, 2016, **28**, 8892-8899.
10. L. Cademartiri, A. Ghadimi and G. A. Ozin, *Acc. Chem. Res.*, 2008, **41**, 1820-1830.
11. L. Cademartiri, G. von Freymann, A. C. Arsenault, J. Bertolotti, D. S. Wiersma, V. Kitaev and G. A. Ozin, *Small*, 2005, **1**, 1184-1187.
12. P. Mohapatra, S. Shaw, D. Mendivelso-Perez, J. M. Bobbitt, T. F. Silva, F. Naab, B. Yuan, X. Tian, E. A. Smith and L. Cademartiri, *Nature Communications*, 2017, **8**, 2038.
13. B. Gehl, U. Leist, V. Aleksandrovic, P. Nickut, V. Zielasek, H. Weller, K. Al-Shamery and M. Baumer, *Rev. Sci. Instrum.*, 2006, **77**.
14. U. Wiedwald, K. Fauth, M. Hessler, H. G. Boyen, F. Weigl, M. Hilgendorff, M. Giersig, G. Schutz, P. Ziemann and M. Farle, *ChemPhysChem*, 2005, **6**, 2522-2526.
15. H. G. Boyen, G. Kastle, F. Weigl, B. Koslowski, C. Dietrich, P. Ziemann, J. P. Spatz, S. Riethmuller, C. Hartmann, M. Moller, G. Schmid, M. G. Garnier and P. Oelhafen, *Science*, 2002, **297**, 1533-1536.
16. J. H. Maurer, L. González-García, B. Reiser, I. Kanelidis and T. Kraus, *ACS Appl. Mater. Interfaces*, 2015, **7**, 7838-7842.
17. E. W. Elliott III, R. D. Glover and J. E. Hutchison, 2015.
18. J. A. Lopez-Sanchez, N. Dimitratos, C. Hammond, G. L. Brett, L. Kesavan, S. White, P. Miedziak, R. Tiruvalam, R. L. Jenkins and A. F. Carley, *Nature Chem.*, 2011, **3**, 551-556.
19. T. M. Squires and S. R. Quake, *Rev. Mod. Phys.*, 2005, **77**, 977-1026.
20. K. J. M. Bishop, C. E. Wilmer, S. Soh and B. A. Grzybowski, *Small*, 2009, **5**, 1600-1630.
21. J. J. De Yoreo, P. U. P. A. Gilbert, N. A. J. M. Sommerdijk, R. L. Penn, S. Whitelam, D. Joester, H. Zhang, J. D. Rimer, A. Navrotsky, J. F. Banfield, A. F. Wallace, F. M. Michel, F. C. Meldrum, H. Cölfen and P. M. Dove, *Science*, 2015, **349**.
22. M. Cargnello, C. Chen, B. T. Diroll, V. V. Doan-Nguyen, R. J. Gorte and C. B. Murray, *J. Am. Chem. Soc.*, 2015, **137**, 6906-6911.
23. R. H. R. Castro, in *Sintering: mechanisms of convention nanodensification and field assisted processes*, eds. R. Castro and K. van Benthem, Springer Science & Business Media, 2012, vol. 35, pp. 1-16.
24. J. P. Kelly and O. A. Graeve, in *Sintering: mechanisms of convention nanodensification and field assisted processes*, eds. R. Castro and K. van Benthem, Springer Science & Business Media, 2012, vol. 35.
25. M. A. Boles, D. Ling, T. Hyeon and D. V. Talapin, *Nat. Mater.*, 2016, **15**, 141.
26. A. M. Smith, L. E. Marbella, K. A. Johnston, M. J. Hartmann, S. E. Crawford, L. M. Kozycz, D. S. Seferos and J. E. Millstone, *Anal. Chem.*, 2015, **87**, 2771-2778.
27. H. G. Boyen, G. Kastle, F. Weigl, P. Ziemann, G. Schmid, M. G. Garnier and P. Oelhafen, *Phys. Rev. Lett.*, 2001, **87**.
28. D. Li, C. Wang, D. Tripkovic, S. Sun, N. M. Markovic and V. R. Stamenkovic, *Acs Catalysis*, 2012, **2**, 1358-1362.
29. D. V. Talapin and C. B. Murray, *Science*, 2005, **310**, 86-89.
30. M. V. Kovalenko, M. Scheele and D. V. Talapin, *Science*, 2009, **324**, 1417-1420.
31. H. G. Boyen, K. Fauth, B. Stahl, P. Ziemann, G. Kastle, F. Weigl, F. Banhart, M. Hessler, G. Schutz, N. S. Gajbhiye, J. Ellrich, H. Hahn, M. Buttner, M. G. Garnier and P. Oelhafen, *Adv. Mater. (Weinheim, Ger.)*, 2005, **17**, 574-+.
32. R. Malakooti, L. Cademartiri, Y. Akcakir, S. Petrov, A. Migliori and G. A. Ozin, *Adv. Mater. (Weinheim, Ger.)*, 2006, **18**, 2189-+.
33. A. Ghadimi, L. Cademartiri, U. Kamp and G. A. Ozin, *Nano Lett.*, 2007, **7**, 3864-3868.
34. U. Kortshagen, *Plasma Chem. Plasma Process.*, 2016, **36**, 73-84.
35. U. R. Kortshagen, R. M. Sankaran, R. N. Pereira, S. L. Girshick, J. J. Wu and E. S. Aydil, *Chem. Rev*, 2016, **116**, 11061-11127.

36. S. Samukawa, M. Hori, S. Rauf, K. Tachibana, P. Bruggeman, G. Kroesen, J. C. Whitehead, A. B. Murphy, A. F. Gutsol and S. Starikovskaia, *J. Phys. D: Appl. Phys.*, 2012, **45**, 253001.
37. J. Lee and D. B. Graves, *Journal of Vacuum Science & Technology A*, 2013, **31**.
38. F. D. Egitto, *Pure and Applied Chemistry*, 1990, **62**, 1699-1708.
39. V. Skurat, *Nuclear Instruments & Methods in Physics Research Section B-Beam Interactions with Materials and Atoms*, 2003, **208**, 27-34.
40. A. C. Fozza, A. Kruse, A. Hollander, A. Ricard and M. R. Wertheimer, *Journal of Vacuum Science & Technology a-Vacuum Surfaces and Films*, 1998, **16**, 72-77.
41. J. Shoeb, M. M. Wang and M. J. Kushner, *Journal of Vacuum Science & Technology A*, 2012, **30**.
42. N. Inagaki, *Plasma Surface Modification and Plasma Polymerization*, CRC Press, Lancaster, PA, 1996.
43. S. Shaw, T. F. Silva, J. M. Bobbitt, F. Naab, C. L. Rodrigues, B. Yuan, J. J. Chang, X. Tian, E. A. Smith and L. Cademartiri, *Chem. Mater.*, 2017, **29**, 7888-7900.
44. S. Shaw, X. C. Tian, T. F. Silva, J. Bobbitt, C. Rodrigues, F. Naab, H. Hamdeh, M. G. Panthani, E. A. Smith and L. Cademartiri, 2018, submitted.
45. P. Mohapatra, D. Mendivelso-Perez, J. M. Bobbitt, S. Shaw, B. Yuan, X. Tian, E. A. Smith and L. Cademartiri, 2018, submitted.
46. C. Jeynes and J. L. Colaux, *Analyst*, 2016, **141**, 5944-5985.
47. M. Mayer, *Nuclear Instruments and Methods in Physics Research Section B: Beam Interactions with Materials and Atoms*, 2014, **332**, 176-180.
48. T. Silva, C. Rodrigues, M. Mayer, M. Moro, G. Trindade, F. Aguirre, N. Added, M. Rizzutto and M. Tabacniks, *Nuclear Instruments and Methods in Physics Research Section B: Beam Interactions with Materials and Atoms*, 2016, **371**, 86-89.
49. A. Schwabedissen, E. C. Benck and J. R. Roberts, *Physical Review E*, 1997, **55**, 3450-3459.
50. U. Cvelbar, N. Krstulovic, S. Milosevic and M. Mozetic, *Vacuum*, 2007, **82**, 224-227.
51. S. Nowak, H. P. Haerri, L. Schlapbach and J. Vogt, *Surface and Interface Analysis*, 1990, **16**, 418-423.
52. M. R. Wertheimer, A. C. Fozza and A. Hollander, *Nuclear Instruments & Methods in Physics Research Section B-Beam Interactions with Materials and Atoms*, 1999, **151**, 65-75.
53. H. Schonhorn and R. H. Hansen, *J. Appl. Polym. Sci.*, 1967, **11**, 1461-1474.
54. K. Pokrovski, K. T. Jung and A. T. Bell, *Langmuir*, 2001, **17**, 4297-4303.
55. P. Calvert and M. Cima, *J. Am. Ceram. Soc.*, 1990, **73**, 575-579.
56. T. L. Hudson, *Growth, diffusion, and loss of subsurface ice on Mars: experiments and models*, California Institute of Technology, 2008.
57. S. Shaw, J. L. Colaux, J. L. Hay, F. C. Peiris and L. Cademartiri, *Adv. Mater. (Weinheim, Ger.)*, 2016, **28**, 8900-8905.